# Experiments with synchronized sCMOS cameras

Iain A. Steele[a], Helen Jermak[a], Chris M. Copperwheat[a], Robert J. Smith[a], Saran Poshyachinda[b], and Boonrucksar Soonthorntham[b]

[a]Astrophysics Research Institute, Liverpool John Moores University, L3 5RF, UK
[b]National Astronomical Research Institute of Thailand, Siripanich Building, 191 Huay Kaew Road, Muang District, Chiangmai, Thailand 50200

## ABSTRACT

Scientific-CMOS (sCMOS) cameras can combine low noise with high readout speeds and do not suffer the charge multiplication noise that effectively reduces the quantum efficiency of electron multiplying CCDs by a factor 2. As such they have strong potential in fast photometry and polarimetry instrumentation. In this paper we describe the results of laboratory experiments using a pair of commercial off the shelf sCMOS cameras based around a 4 transistor per pixel architecture. In particular using a both stable and a pulsed light sources we evaluate the timing precision that may be obtained when the cameras readouts are synchronized either in software or electronically. We find that software synchronization can introduce an error of $\sim$ 200-msec. With electronic synchronization any error is below the limit ($\sim$ 50-msec) of our simple measurement technique.

**Keywords:** CMOS, sCMOS, fast photometry, polarimetry, time domain astrophysics, detectors

## 1. INTRODUCTION

Fast readout optical imaging sensors have many applications in modern observational astrophysics. For example they are key elements in adaptive optic system wavefront sensors,[1] lucky imaging systems,[2] fast photometers[3] and optical ring polarimeters.[4,5]

In many of these applications, it is desirable to operate multiple cameras in a synchronized fashion. For example in order to allow simultaneous observations at multiple wavelengths the beam is often split by dichroic mirrors. Examples of instruments of this sort include the ULTRACAM[3] fast imaging photometer and the RINGO3[5] fast imaging polarimeter. In addition we have proposed a novel design of imaging polarimeter (MOPTOP[6]) where the Stokes $q$ and $u$ parameters can be calculated from difference images between two simultaneously read out cameras. In in this last case any error in the synchronization of the camera readouts will translate directly into a systematic error in the measured polarimetry.

Traditionally fast imaging photometry has been accomplished using frame transfer CCDs and in more recent years electron multiplying CCDs (EMCCDs[7]). Electron multiplying CCDs add to the fast readout time of a conventional frame transfer CCD a charge multiplication register in the output circuit. This reduces the readout noise of the detector to single electron values. However, a disadvantage of EMCCDs is the charge multiplication noise which is added by this process. This increases the photon counting noise of the detector by a factor $\sim \sqrt{(2)}$, which is equivalent to a quantum efficiency reduction by a factor of 50%.

The recent emergence of commercial cameras based on scientific CMOS (sCMOS) technology offers another possible technology for fast readout applications. sCMOS detectors are engineered for low readout noise and high quantum efficiency. They are active pixel sensors, with readout and multiplex circuitry associated with each pixel. The two main architectures are 4-transistor per pixel (4T) and 5-transistor per pixel (5T). In general terms, the 4T architecture provides higher quantum efficiency but does not have a "global" reset. This means that "rolling shutter" effects will be present that give different exposure start times for different regions of the image (the total exposure time for each pixel is unaffected however). The 5T architecture provides a true

Further author information: (Send correspondence to IAS)
IAS: E-mail: I.A.Steele@ljmu.ac.uk

High Energy, Optical, and Infrared Detectors for Astronomy VII, edited by Andrew D. Holland, James Beletic,
Proc. of SPIE Vol. 9915, 991522 · © 2016 SPIE · CCC code: 0277-786X/16/$18 · doi: 10.1117/12.2232349

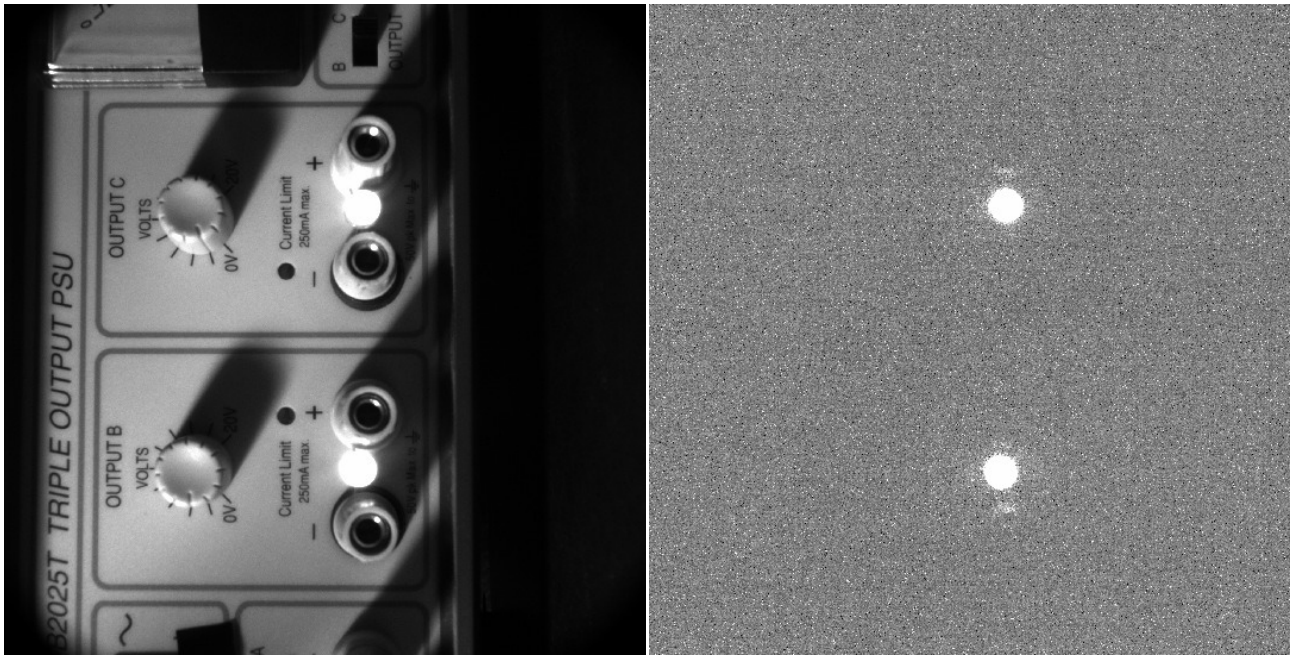


Figure 1. Experimental setup for generating a pair of artificial stars. Each red LED "star" is powered by an independent voltage regulated circuit of the power supply. The left hand image shows a 0.1 second exposure illuminated by a 15W red desk lamp. The "stars" are completely saturated. The right hand image shows the effect of placing a UG1 filter in front of the camera lens and operating the setup in darkness. The background is now featureless and the stars have average counts $\sim 2500$ per pixel.

photometric electronic "shutter" over the whole field at the expense of lower quantum efficiency and higher read noise.

In this paper we investigate the synchronization that can be achieved between a pair of commercial sCMOS cameras. In particular we compare the accuracy of synchronization that can be obtained using software versus electronic approaches to synchronization.

## 2. METHOD

We chose to investigate the synchronization performance of the a pair of cameras are manufactured by Andor. The model is "Zyla 4.2 plus" with $2048 \times 2048$ active pixels. This is a 4T design, and has low read noise ($\sim 1e^-$) and high quantum efficiency (peak $\sim 82\%$ at 5700-Å). We used the USB 3.0 version of the camera, which has a maximum frame rate of 40-Hz at 16-bit readout depth. The standard readout mode is bi-directional and symmetrical about the detector centre line (i.e. the top half of the detector reads out "upwards" while the bottom half simultaneously reads out "downwards").

Readout software was written in C using the Linux version of the Andor SDK 3.11. The host computer was equipped with an Intel i7 CPU with 8GB RAM and a 64 GB solid state disk. Both cameras were connected to the same host computer via a USB 3.0 hub. The software was written to store all images as part of a sequence in the computer RAM until readout was complete. Only once readout was complete was any data written to disk. This limited the maximum length of a sequence to $\sim 500$ frames, but avoided introducing delays due to disk buffering into the readout sequence. In an operational environment, it is likely that a multi-threaded circular buffer approach would be necessary if longer sequences were required.

The cameras were operated cooled to $0^\circ$ C. For the exposure lengths used in our experiments ($< 2$ seconds) this meant that the average dark current was $< 1e^-$ per pixel. The "bad pixel mask" and "noise suppression" features of the cameras were disabled due to their uncertain effect on the photometric quality.

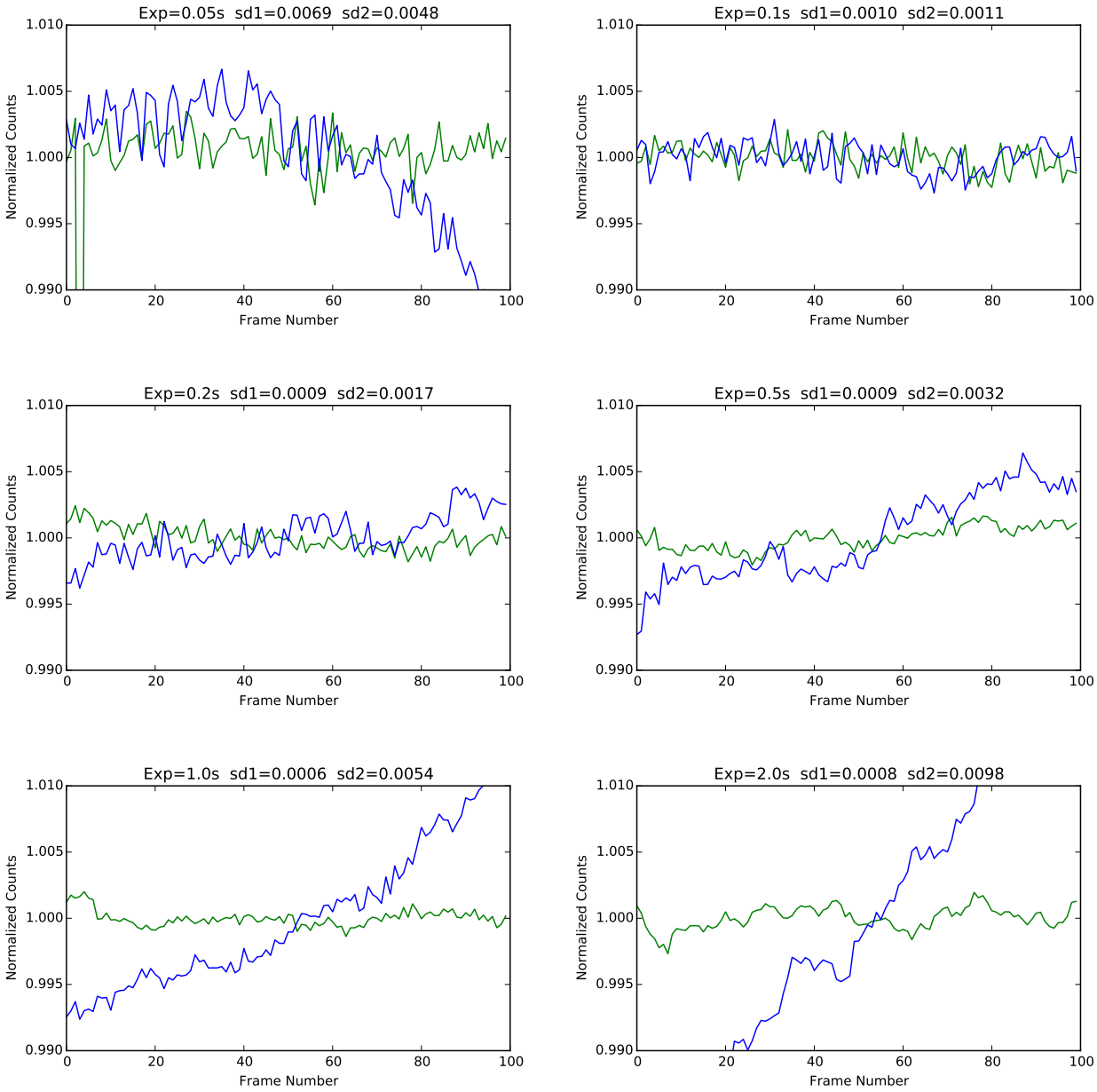


Figure 2. Normalized "light curves" for two artificial stars in the field of view of a single detector. Each light curve consists of 100 frames. Exposure timing is controlled by software. The exposure times range from 0.05 to 2.0 seconds. The green curve is "star 1" and the blue curve "star 2". The exposure time and standard deviation for each star are given above each plot.

All experiments were carried out in a dark room. Each camera ("A" and "B") was equipped with a commercial 25-mm focal length C-mount camera lens that was operated at minimum aperture ($f/16$) to reduce the system sensitivity. In addition a UG1 filter in front of each lens reduced sensitivity still further. As a light sources we used standard commercial red light emitting diodes (LEDs) to produce artificial stars. For initial testing we used a pair of LEDs powered by a dual regulated power supply (Figure 1). In order to avoid introducing uncertainties into our analysis due to the rolling shutter the cameras were aligned such that the two artificial stars ("1" and

"2") lay symmetrically about the detector centre line and hence had the same start exposure time. For the later tests we used a signal generator to drive a single LED and thereby provide a variable light source.

## 3. RESULTS: SOFTWARE SYNCHRONIZATION

In this section we will discuss our results using the cameras with software control of exposure timing. In this mode using the Andor SDK the exposure length and number of exposures for each camera can be specified. Each detector can then be placed in Acquisition mode, where it will take the requested series of exposures. Progress can be monitored by a callback that indicates when the memory buffer associated with each exposure is filled. When all buffers have been filled by both cameras, the Acquisition mode is ended and the data is written to disk as a series of FITS files (one per frame per camera).

### 3.1 Single Camera, Two Stable Stars

For our initial experiments we used a single camera to view two artificial stars of nominally constant brightness. We observed light curves of 100 frames at exposure times of 0.05, 0.1, 0.2, 0.5, 1.0 and 2.0 seconds. Photometry of each frame was carried out using the aperture photometry mode of the `Sextractor` software package. The resulting light curves are presented in Figure 2.

From Figure 2 it can be seen that star 1 is considerably more stable than star 2 on longer time scales. A Spearman rank correlation test indicates no correlated variability between stars 1 and 2 is detected. We therefore attribute the difference in variability between the two sources to drift in the power supply for star B rather than any exposure length variation between the frames. The short time scale ($< 10$ frame) variability of stars 1 and 2 is similar. For all exposure times the standard deviation of star 1 is similar (neglecting the 0.05 second exposure which is affected by a single bad measurement) at $\sim 0.008$. This is encouraging, indicating that a photometric precision of better than $\sim 1\%$ is apparently straightforward to achieve with the detector (neglecting any potential non-linearities that are not detected with this method).

### 3.2 Two Cameras, Two Stable Stars

For our next experiments we aligned both cameras (A and B) to observe both stars 1 and 2. We used exposure times of 0.1, 0.2 and 0.4 seconds. The resulting light curves are presented in Figure 3. The left hand plots are the results for star 1, and the right hand side for star 2. In this case both stars show longer timescale variability. The variability is well correlated on longer timescales between the two cameras. Star 2 shows more short timescale variability than star 1 in both cameras. Careful examination of the star 2 lightcurves shows an apparent lag between cameras A and B. For example for the 0.1 second exposures, the camera A lightcurve appears to lead the camera B lightcurve by 2 frames. In order to investigate this, we carried out a cross correlation analysis on the two camera lightcurves. The results of this are presented below each lightcurve in Figure 3. It can be seen that a lag of 2 frames is found for the 0.1 second exposures, 1 frame for the 0.2 second exposures and $\sim 0.5$ frame for the 0.4 second exposure. It therefore appears that there is a roughly constant time offset in exposure start time between the two cameras of $\sim 200$ msec when using software synchronization.

### 3.3 Two Cameras, One Variable Star

In order to more fully investigate the apparent lag between the two cameras found in the previous section, we replaced our pair of "stable" artificial stars with a single star driven by a signal generator operating at $\sim 1$ Hz. This provided a strongly pulsed signal. The resulting light curves from the two cameras are presented in Figure 4. The 2 frame ($\sim$ 200-msec) lag is obvious in both the light curve and the cross correlation results.

## 4. RESULTS: FREE-RUNNING ELECTRONIC SYNCHRONIZATION

In this section we will discuss our results of using the cameras with hardware control of exposure timing. In this mode using the Andor SDK the exposure length and start is defined by an electronic TTL level signal fed to the camera. The exposure starts on a high state transition of the `TRIGGER` line, and ends when the line transitions back to the low state. We used a signal generator to provide a square wave `TRIGGER` signal with a frequency of

10Hz. This will give an exposure cadence of 0.1 seconds with an exposure time of 0.05 seconds (due to the 50:50 duty cycle of the simple square wave trigger used).

As per software readout, the start of the exposure sequence is defined when the SDK is used to place each camera in Acquisition mode. We therefore call this mode "free-running" as the start of the exposure sequence is not defined by the continuously pulsed `TRIGGER` signal. Progress can be monitored by a callback that indicates when the memory buffer associated with each exposure is filled. When all buffers have been filled by both cameras, the Acquisition mode is ended and the data is written to disk as a series of FITS files (one per frame per camera).

We carried out our investigation of this mode of operation by making observations using Cameras A and B of our pulsed light source. (i.e. as Section 3.3 but with the free running `TRIGGER` signal). A typical resulting light curves and associated cross correlation is presented in Figure 5. In the example presented the lag is the lag is 3 frames (i.e. $\sim 300$ msec), however lags of 2 frames were also obtained in different runs. Overall the lag is the similar to the the value obtained using software synchronization. It therefore seems apparent that this lag is caused by a time difference of that order between the switching of the two cameras into acquisition mode rather than by timing difference during acquisition between software and hardware timing. In both cases this switch to acquisition mode is carried out by two identical SDK commands issued immediately sequentially to one another by out software. We note a possible solution may be to issue the commands simultaneously in two separate threads, although the success or otherwise of this would depend on the nature of the threading within the SDK and the USB communications with the two cameras.

On the positive side, we note that the form of the correlation peak is much sharper in this case than in the software controlled case (compare Figures 4 and 5). This implies that the offset is likely an exact integer multiple of the number of frames in this electronically free running triggered mode, whereas in the software case the offset can be any value. This is as expected when the start time of the individual exposures on both cameras is controlled by the same trigger signal. The tight correlation also implies that there is little jitter in individual exposure lengths.

## 5. RESULTS: TRIGGERED ELECTRONIC SYNCHRONIZATION

Given the conclusion of the previous section that the lag between the two cameras was caused by a delay between the switching of the two cameras into acquisition mode, we therefore modified our hardware triggering setup. In the modified version, a time delay of 1 second between putting the two cameras into acquisition mode and the start of the pulse signal being fed to the cameras was introduced. A typical resulting light curve and cross correlation analysis is presented in Figure 6. No lag between frames was apparent in repeated tests and the cross correlation peak is again very sharp, indicating that sub-frame deviations are likely to be very small. It therefore appears that delaying the application of the hardware trigger to the camera for $\sim 1$ second (the exact time was not determined) synchronizes the start time of the exposures to better than 1 frame. Given the exposure time of 50ms in this mode, we are confident that this is a reasonable upper limit to the degree of synchronization obtained, although we suspect it is far better than that.

## 6. SUMMARY AND CONCLUSIONS

We have carried out a simple set of experiments to determine how well the readout of two commercial off-the-shelf scientific CMOS cameras may be synchronized using a pair of stable and a single pulsed light source. We found that in software controlled mode, the cameras were capable of photometric performance better than 1%. However in such a mode we found the a delay in start time between the two cameras of $\sim$ 200-msec. The lag was apparently not an exact multiple of exposure time.

We then experimented with synchronizing the two camera exposures electronically using a simple free running external clock to drive exposure timing. In this case we still found lags were present of $200 - 300$-msec, although in this case they were apparently an exact multiple of the exposure time. By experimentation we found that by delaying the application of the start clock trigger signal to $\sim$1 second after putting the cameras into acquisition mode we no longer able to detect any lags between the cameras to the $\sim$ 50-msec precision of our simple experimental technique. We plan to investigate the exact lag in this mode of operation in a future set of experiments using a more structured variable light-source and longer time series.

## ACKNOWLEDGMENTS

This work was partially supported by the UK Newton Fund via the Science and Technologies Facilities Council.

## REFERENCES

[1] Hickson, P. and Burley, G., "Single-image wavefront curvature sensing," in [*Adaptive Optics in Astronomy*], Ealey, M. A. and Merkle, F., eds., *Proc SPIE* **2201**, 549–554 (May 1994).

[2] Law, N. M., Mackay, C. D., and Baldwin, J. E., "Lucky imaging: high angular resolution imaging in the visible from the ground," *Astronomy and Astrophysics* **446**, 739–745 (Feb. 2006).

[3] Dhillon, V., Marsh, T. R., Kelly, J., Pashley, R., Stevenson, M., Atkinson, D., Beard, S., Ives, D., Peacocke, T., Tierney, C., and Vick, A., "ULTRACAM – an ultra-fast, triple-beam CCD camera," in [*The Physics of Cataclysmic Variables and Related Objects*], Gänsicke, B. T., Beuermann, K., and Reinsch, K., eds., *Astronomical Society of the Pacific Conference Series* **261**, 672 (Jan. 2002).

[4] Steele, I. A., Bates, S. D., Guidorzi, C., Mottram, C. J., Mundell, C. G., and Smith, R. J., "RINGO2: an EMCCD-based polarimeter for GRB followup," in [*Ground-based and Airborne Instrumentation for Astronomy III*], *Proc SPIE* **7735**, 773549 (July 2010).

[5] Arnold, D. M., Steele, I. A., Bates, S. D., Mottram, C. J., and Smith, R. J., "RINGO3: a multi-colour fast response polarimeter," in [*Ground-based and Airborne Instrumentation for Astronomy IV*], *Proc SPIE* **8446**, 84462J (Sept. 2012).

[6] Jermak H. et al., "MOTOP: a multi-colour optimized optical polarimeter," *Proc SPIE, this conference* (2016).

[7] Smith, N., Coates, C., Giltinan, A., Howard, J., O'Connor, A., O'Driscoll, S., Hauser, M., and Wagner, S., "EMCCD technology and its impact on rapid low-light photometry," in [*Optical and Infrared Detectors for Astronomy*], Garnett, J. D. and Beletic, J. W., eds., *Proc SPIE* **5499**, 162–172 (Sept. 2004).

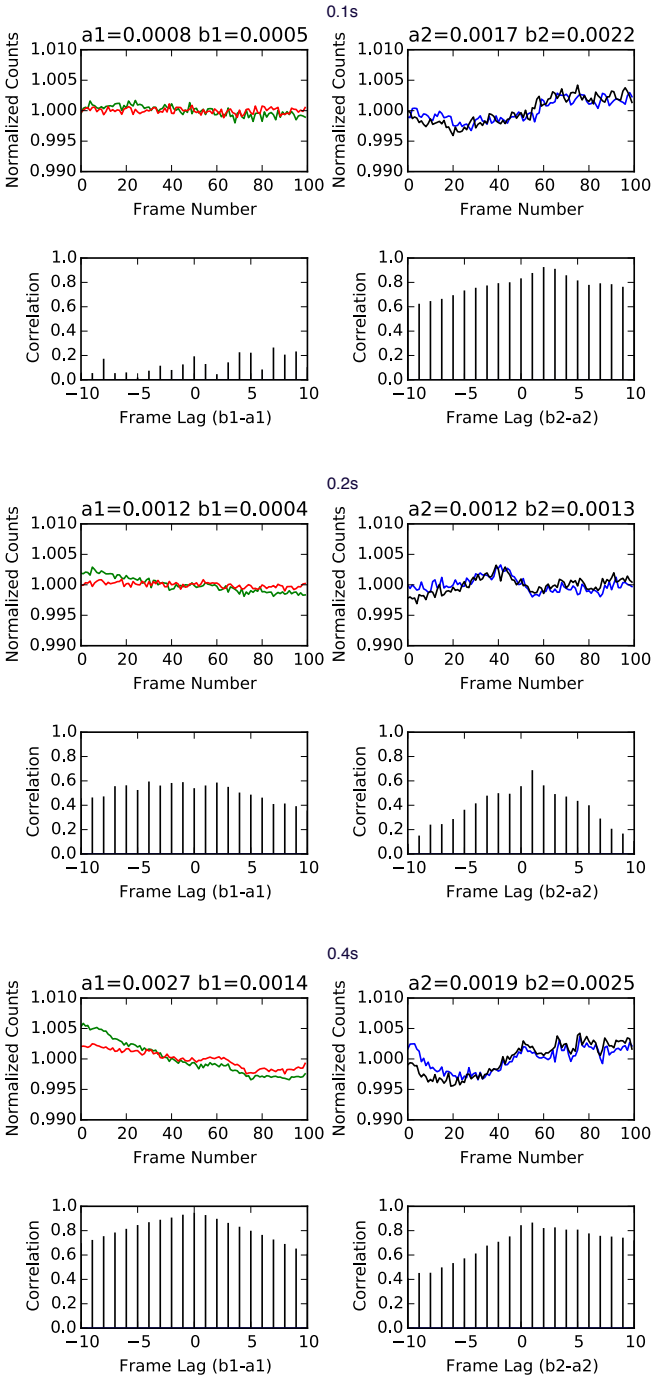


Figure 3. Normalized "light curves" for two artificial stars in the field of view of a pair of detectors. Each light curve consists of 100 frames. Exposure timing is controlled by software. The exposure times from top to bottom are 0.1, 0.2 and 0.4 seconds. The left hand panels relate to observations of "star 1" with cameras A (green curve) and B (red curve). The right hand panels related to observations of "star 2" with cameras A (blue curve) and B (black curve). The title of each light curve gives the standard deviation for the two different camera observations of that object. Below each light curve is a cross-correlation plot for lags between -10 and +10 frames between cameras B and A.

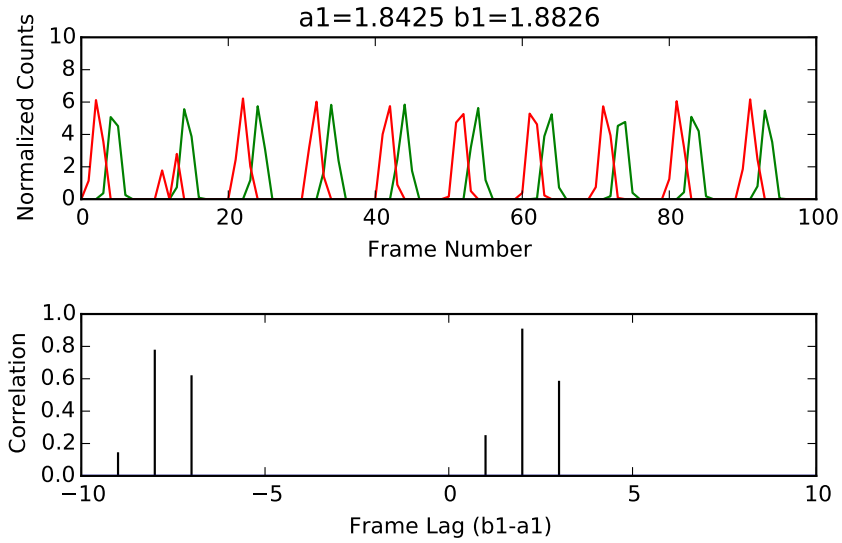


Figure 4. Normalized "light curves" for a single pulsed artificial star generated in field of view of a a pair of detectors (camera A = green curve, camera B = red curve). Each light curve consists of 100 frames. The 0.1 second exposure time was controlled by software. The title above the light curve gives the standard deviation for the two different camera observations of that object. Below the light curve is a cross-correlation plot for lags between -10 and +10 frames between cameras B and A.

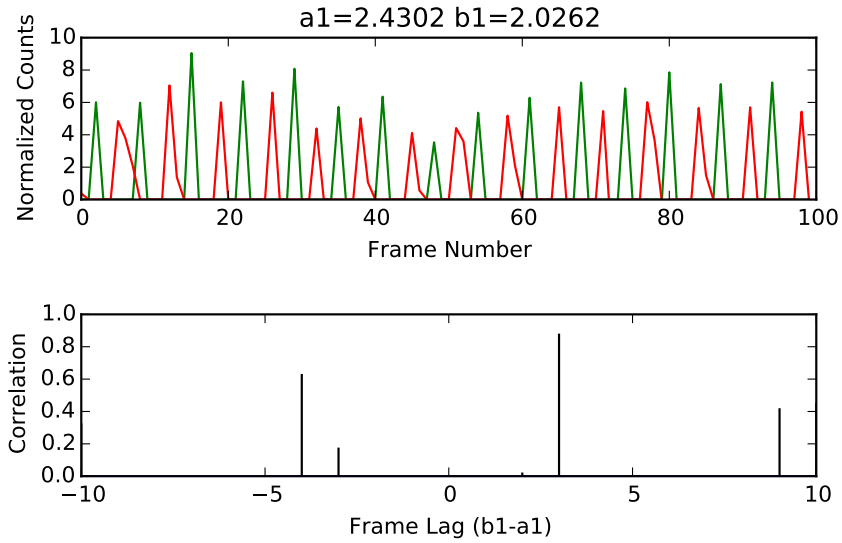


Figure 5. Normalized "light curves" for a single pulsed artificial star generated in field of view of a a pair of detectors (camera A = green curve, camera B = red curve). Each light curve consists of 100 frames. The 0.1Hz exposure cadence second exposure time was controlled by a free running hardware trigger signal generated by a signal generator running at 10Hz. The title above the light curve gives the standard deviation for the two different camera observations of that object. Below the light curve is a cross-correlation plot for lags between -10 and +10 frames between cameras B and A.

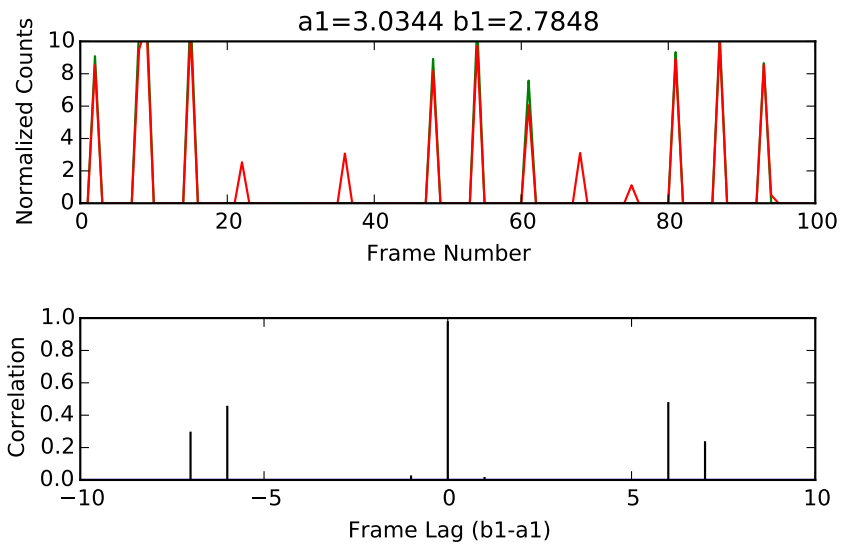


Figure 6. Normalized "light curves" for a single pulsed artificial star generated in field of view of a a pair of detectors (camera A = green curve, camera B = red curve). Each light curve consists of 100 frames. The 0.1Hz exposure cadence second exposure time was controlled by a hardware trigger signal generated by a signal generator running at 10Hz. The trigger signal was activated one second after the API commands were issued to place each cameras into its Acquisition Mode. The title above the light curve gives the standard deviation for the two different camera observations of that object. Below the light curve is a cross-correlation plot for lags between -10 and +10 frames between cameras B and A.